ROZPRAWY INŻYNIERSKIE • ENGINEERING TRANSACTIONS • 32, 2, 211—223, 1984
Polska Akademia Nauk • Instytut Podstawowych Problemów Techniki

AXISYMMETRIC STATIC AND DYNAMIC BUCKLING OF ORTHOTROPIC SHALLOW SPHERICAL CAPS WITH INITIAL IMPERFECTIONS

P.C. DUMIR, M.L. GANDHI and Y. NATH (NEW DELHI)

This study deals with the static and dynamic axisymmetric buckling of elastic orthotropic thin spherical caps with initial imperfections. A simple type of axisymmetric imperfection is considered. The governing equations are formulated in terms of normal displacement w and stress function ψ. The orthogonal point collocation method is used for spatial discretization and the Newmark-β scheme is used for time-marching. The uniformly distributed static and step function pressure loads are considered in this study. The solutions of perfect spherical caps under step loading are in good agreement with previous findings. The influence of initial imperfections on the static and dynamic buckling loads of isotropic and orthotropic shallow spherical caps has been investigated for the shell rise to thickness ratio up to ten.

NOTATION

a, h radius of the base of the cap and thickness,
H, R apex height and radius of the spherical cap,
$\lambda = 2\,[3\,(1-\nu_\theta^2)]^{1/4}\,(H/h)^{1/2}$ shell parameter,
E_r, E_θ; ν_r, ν_θ elastic moduli; Poisson's ratios,
γ mass density,
$\beta = E_\theta/E_r$ orthotropic parameter,
t, τ time, nondimensional time,
D $E_\theta\, h^3/12\,(\beta-\nu_\theta^2)$,
w^*, u^*; ψ^* normal and inplane displacements; stress function,
w, u; ψ nondimensional displacements, stress function,
w_0^* initial position of the middle surface of the spherical cap above the base,
w_i^*, w_i initial imperfection, nondimensional initial imperfection,
w_{i0} initial imperfection at the apex,
r, ρ radius, nondimensional radius,
q uniformly distributed pressure load,
$P = [3\,(1-\nu_\theta^2)]^{1/2}\,\dfrac{qa^4}{8E_r\,h^4}\left(\dfrac{h}{H}\right)^2$ nondimensional load,
$\overline{w}, \overline{w}_{\max}$ average deflection, maximum average deflection,
P_{cr} buckling load,
N_r, N_θ inplance forces,
M_r, M_θ bending moments,
Q_r transverse shear,
$\varepsilon_r, \varepsilon_\theta$ strains,
$\sigma_r^*, \sigma_\theta^*$ stresses,
α, δ parameters of Newmark-β scheme,

$\Delta\tau$ time step,
$(\,)', (\dot{})$ differentiation with respect to ρ and τ,
N, ρ_i number and radii of collocation points,
a_i, b_i coefficients of power series expansion of w and ψ,
A_1, A_2, A_3 coefficients in quadratic extrapolation,
Subscript J step of marching,
Subscripts p, i predicted value, value at the i-th collocation point.

1. Introduction

Nonlinear axisymmetric static and dynamic buckling of elastic shallow thin spherical caps have been intensively studied [1–11]. Most of these studies consider clamped perfectly spherical isotropic caps. For a more realistic prediction of the load carrying capacity of these shells employed in practice, the effect of initial imperfections should be considered. The practical manufacturing and assembling techniques always result in some deviation from the ideal geometrical configuration of the shell. The initial imperfection so induced is regarded as a major factor to lower the load-carrying capacity for shallow-spherical shells and partly explains the discrepancy between experimental data and theoretical solutions for perfect shells. Budiansky [1] and Uemura [8] have presented static load-deflection response and buckling of isotropic shallow spherical caps with axisymmetric initial imperfections in the form of the deflected shape of clamped circular plate under uniformly distributed load. Koga and Hoff [4] gave the value of static buckling pressure for isotropic complete spherical shells with dimple type imperfections. Kao *et al.* [10, 11] analysed the effect of initial imperfections on the static and dynamic buckling loads of isotropic elastic and elastic-plastic shallow spherical shells for few values of the shell parameter λ.

The object of this study is to investigate the effect of initial imperfections on the axisymmetric static and dynamic buckling loads of orthotropic shallow spherical shells subjected to uniformly distributed load for apex rise to thickness ratio of the shell (H/h) from 2 to 10. The dynamic load considered is a step function load. This work is restricted to axisymmetric buckling since it is critical in a certain range of shell parameters and the understanding of symmetric buckling is the first step even when asymmetric behaviour is critical.

The governing equations for the axisymmetric response of a cylindrically orthotropic shallow spherical shell with initial imperfection are formulated in terms of normal displacement w and stress function ψ. The normal displacement w and stress function ψ are expanded in finite power series. The orthogonal point collocation method is used for space-wise discretization and the Newmark-β scheme for time-marching. Detailed convergence studies have revealed that for the range of shell parameters considered in this study ($H/h \leqslant 10$), nine collocation points and $\Delta\tau = 0.002$ lead to accurate results. As an additional check on the accuracy of results, at every step the sum of the kinetic and strain energy of the cap is compared with the sum of the initial kinetic energy and the external work done up to that step. It has been found that this balance of energy has been maintained very well at all steps.

The present isotropic results are in good agreement with the available results. New static and dynamic buckling results are presented for orthotropic shallow spherical caps with initial imperfections.

2. Mathematical formulation

The middle surface of a shallow spherical cap (Fig. 1) can be approximated by the paraboloid

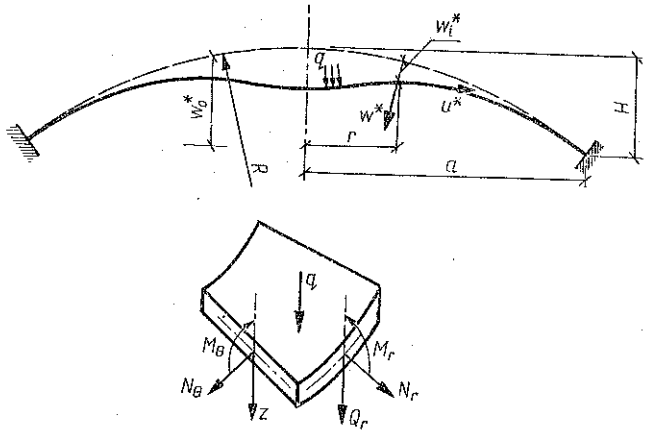

FIG. 1. Geometry and free body diagram for axisymmetric clamped spherical cap with initial imperfections.

$$w_0^*=H\left[i-\left(\frac{r}{a}\right)^2\right], \tag{2.1}$$

where a is the base radius and H is the rise of the middle surface at the apex. The radius of curvature R of the shell is

$$R=a^2/2H. \tag{2.2}$$

Neglecting inplane and rotary inertia, the equilibrium equations for inplane stress resultants and moments are

$$\begin{aligned}(rN_r)_{,r}-N_\theta&=0,\\ (rM_r)_{,r}-M_\theta-rQ_r&=0.\end{aligned} \tag{2.3}$$

If w_i^* is the initial imperfection, the equation of motion in the normal direction is

$$[rN_r\,(w^*+w_i^*-w_0^*)_{,r}+rQ_r]_{,r}+rq=\gamma hrw^*_{,tt}. \tag{2.4}$$

This can be integrated from 0 to r to yield

$$rN_r\,(w^*+w_i^*-w_0^*)_{,r}+rQ_r=-\int_0^r r\,(q-\gamma hw^*_{,tt})\,dr. \tag{2.5}$$

Neglecting normal shear strains, the strain-displacement relations for moderately large deflections are

$$\varepsilon_r = u^*_{,r} - \frac{w^*}{R} + \frac{1}{2} w^{*2}_{,r} - z w^*_{,rr} + w^*_{i,r} w^*_{,r}$$

$$\varepsilon_\theta = \frac{u^*}{r} - \frac{w^*}{R} - \frac{z}{r} w^*_{,r}. \tag{2.6}$$

For cylindrical orthotropy, the constitutive equations are

$$\varepsilon_r = \frac{\sigma_r}{E_r} - \nu_\theta \frac{\sigma^*_\theta}{E_\theta}, \qquad \sigma^*_r = \frac{E_\theta}{\beta - \nu_\theta^2}(\varepsilon_r + \nu_\theta \varepsilon_\theta),$$

$$\varepsilon_\theta = \frac{\sigma^*_\theta}{E_\theta} - \nu_r \frac{\sigma^*_r}{E_r}, \qquad \sigma^*_\theta = \frac{E_\theta}{\beta - \nu_\theta^2}(\nu_\theta \varepsilon_r + \beta \varepsilon_\theta), \tag{2.7}$$

where

$$\beta = \frac{E_\theta}{E_r}, \qquad \frac{\nu_r}{E_r} = \frac{\nu_\theta}{E_\theta}.$$

The stress resultants are given by

$$N_r = \int_{-h/2}^{h/2} \sigma^*_r \, dz = \frac{E_\theta h}{\beta - \nu_\theta^2}\left[u^*_{,r} - \frac{w^*}{R} + \frac{1}{2} w^{*2}_{,r} + w^*_{i,r} w^*_{,r} + \nu_\theta\left(\frac{u^*}{r} - \frac{w^*}{R}\right)\right],$$

$$N_\theta = \int_{-h/2}^{h/2} \sigma^*_\theta \, dz = \frac{E_\theta h}{\beta - \nu_\theta^2}\left[\nu_\theta\left(u^*_{,r} - \frac{w^*}{R} + \frac{1}{2} w^{*2}_{,r} + w^*_{i,r} w^*_{,r}\right) + \beta\left(\frac{u^*}{r} - \frac{w^*}{R}\right)\right]. \tag{2.8}$$

The moments are given by

$$M_r = \int_{-h/2}^{h/2} z\sigma^*_r \, dz = -D\left[w^*_{,rr} + \frac{\nu_\theta}{r} w^*_{,r}\right],$$

$$M_\theta = \int_{-h/2}^{h/2} z\sigma^*_\theta \, dz = -D\left[\nu_\theta w^*_{,rr} + \frac{\beta}{r} w^*_{,r}\right], \tag{2.9}$$

where

$$D = E_\theta h^3/12(\beta - \nu_\theta^2).$$

Equation (2.3) can be satisfied if stress resultants are expressed in terms of a stress function ψ^* as follows:

$$N_r = \psi^*/r, \qquad N_\theta = \psi^*_{,r}. \tag{2.10}$$

Substituting Q_r from Eq. (2.3) into Eq. (2.5) and making use of Eqs. (2.1), (2.9) and (2.10), the equation of motion becomes

$$D\left[r w^*_{,rrr} + w^*_{,rr} - \frac{\beta}{r} w^*_{,r}\right] - \psi^*\left(w^*_{,r} + w^*_{i,r} + \frac{ZHr}{a^2}\right) = \int_0^r r(q - rhw^*_{,tt})\, dr. \tag{2.11}$$

Eliminating u^* from Eq. (2.8) and using Eqs. (2.2) and (2.10), the compatibility equation can be expressed as

$$r\psi^*_{,rr}+\psi_{,r}-\frac{\beta}{r}\psi^*+\frac{hE_\theta}{2}w^*_{,r}\left[w^*_{,r}+\frac{4Hr}{a^2}+2w_{i,r}\right]=0. \tag{2.12}$$

Introducing the following dimensionless parameters

$$w=\frac{w^*}{h},\quad \psi=\frac{a\psi^*}{D},\quad \rho=\frac{r}{a},$$
$$w_i=\frac{w^*_i}{h},\quad \tau=\left[\frac{D}{\gamma h a^4}\right]^{1/2}t, \tag{2.13}$$
$$P=\frac{\lambda^2 a^4 q}{32E_r H^3 h}=[3(1-\nu_\theta^2)]^{1/2}\left(\frac{h}{H}\right)^2\frac{qa^4}{8E_r h^4}$$

the governing equations (2.10) and (2.12) reduce to the following dimensionless form:

$$\rho^2 w'''+\rho w''-\beta w'-\rho\psi\left(w'+w'_i+\frac{2H}{h}\rho\right)=$$
$$=\rho\int_0^\rho\left[\frac{96(\beta-\nu_\theta^2)}{\beta\{3(1-\nu_\theta^2)\}^{1/2}}\left(\frac{H}{h}\right)^2 P-\ddot{w}\right]\rho\,d\rho, \tag{2.14}$$
$$\rho^2\psi''+\rho\psi'-\beta\psi+6(\beta-\nu_\theta^2)\rho w'\left(w'+\frac{4H}{h}\rho+2w'_i\right)=0,$$

where $(\,)'$ and $\dot{(\,)}$ are derivatives with respect to ρ and τ, respectively. The initial conditions are assumed as $w(\rho,0)=\dot{w}(\rho,0)=0$.

The boundary conditions at the centre and outer immovable clamped edge are

$$\begin{aligned}&\rho=0:\quad w'(0)=0,\quad \psi(0)=0,\\ &\rho=1:\quad w(1)=0,\quad w'(1)=0,\quad \psi'(1)-\nu_\theta\psi(1)=0.\end{aligned} \tag{2.15}$$

The axisymmetric imperfection adopted in this study is of the dimple type which was also used in [4, 10, 11]. This type of imperfection is expressed mathematically as

$$w_i=w_{i0}(1-\rho^2)^3, \tag{2.16}$$

where

$$w_{i0}=w^*_i(0)/h$$

is the maximum imperfection which occurs at the shell apex.

3. Method of solution

The time is incremented in small steps $\Delta\tau$ and the nonlinear Eqs. (2.14) are solved iteratively at step J by linearizing them for each iteration by writing the nonlinear terms as

$$(\psi w')_J=w'_{J_p}\psi_J,\quad (w')^2_J=w'_{J_p}w'_J. \tag{3.1}$$

where the predicted term w'_{J_p} is taken as the mean of the previous two iterations. For the first iteration, the predicted value is extrapolated quadratically from the values at three previous steps,

$$w'_{J_p}=A_1\,(w'_{J-1})+A_2\,(w'_{J-2})+A_3\,(w'_{J-3}), \tag{3.2}$$

where A_1, A_2, A_3 for the different stages are: $1, 0, 0$ $(J=1)$; $2, -1, 0$ $(J=2)$; and $3, -3, 1$ $(J\geqslant 3)$. The orthogonal point collocation method is used for spatial discretization. For N collocation points w and ψ are expanded as polynomials in ρ,

$$w(\rho)=\sum_{m=1}^{N+3}\rho^{m-1}\,a_m, \qquad \psi(\rho)=\sum_{n=1}^{N+2}\rho^{n-1}\,b_n, \qquad 0\leqslant\rho\leqslant 1. \tag{3.3}$$

The differential equations (2.14) are collocated at the zeros of the Nth order Legendre polynomial in the range 0 to 1. The inertia term in Eq. (2.14) is discretized using the Newmark-β scheme with parameters corresponding to the average acceleration method [12]

$$\ddot{w}_J=\frac{w_J-w_{J-1}}{\alpha\,(\Delta\tau)^2}-\frac{\dot{w}_{J-1}}{\alpha\,(\Delta\tau)}-\left(\frac{0.5}{\alpha}-1\right)\ddot{w}_{J-1} \tag{3.4}$$

with

$$\dot{w}_J=\dot{w}_{J-1}+[(1-\delta)\,\ddot{w}_{J-1}+\delta\ddot{w}_J]\,(\Delta\tau),$$
$$w_J=w_{J-1}+\dot{w}_{J-1}\,(\Delta\tau)+[(0.5-\alpha)\,\ddot{w}_{J-1}+\alpha\ddot{w}_J]\,(\Delta\tau)^2.$$

The collocation equations for differential equations (2.14) are:

$$\sum_{m=1}^{N+3}\left[(m-1)\,\rho_i^{m-2}\,\{(m-2)^2-\beta\}+\frac{1}{\alpha\,(\Delta\tau)^2\,(m+1)}\,\rho_i^{m+2}\right]a_m-$$
$$-\sum_{n=1}^{N+2}\left[(w'_{J_p})_i-6w_{i0}\,\rho_i\,(1-\rho_i^2)^2+\frac{2H}{h}\,\rho_i\right]\rho_i^n\,b_n=\frac{48\,(\beta-\nu_\theta^2)}{\beta\,[3\,(1-\nu_\theta^2)]^{1/2}}\times$$
$$\times\left(\frac{H}{h}\right)^2\rho_i^3\,P_J+\rho_i\int_0^{\rho_i}\left[\frac{w_{J-1}}{\alpha\,(\Delta\tau)^2}+\frac{\dot{w}_{J-1}}{\alpha\,(\Delta\tau)}+\left(\frac{0.5}{\alpha}-1\right)\ddot{w}_{J-1}\right]\rho\,d\rho, \tag{3.5}$$

$$\sum_{m=1}^{N+3}[6\,(\beta-\nu_\theta^2)\,(m-1)]\,\rho_i^{m-1}\left\{(w'_{J_p})_i+\frac{4H}{h}\,\rho_i-12w_{i0}\,\rho_i\,(1-\rho_i^2)^2\right\}a_m+$$
$$+\sum_{n=1}^{N+2}\rho_i^{n-1}\,[(n-1)^2-\beta]\,b_n=0, \qquad i=1, \ldots, N.$$

The five equations for boundary conditions are solved for a_1, a_2, a_3 and b_1, b_2 in terms of the remaining N a and b, respectively. Equations (3.5) are the $2N$ discretized equations for the coefficients a and b. The iterations are continued until $w(0)$, $\psi'(0)$ and $\psi'(1)$ satisfy a relative convergence criterion within 0.1% accuracy. After getting the converged solution for the coefficients a and b at step J, the procedure is repeated for the $(J+1)$-th step.

3.1. Dynamic buckling

The criteria suggested by BUDIANSKY and ROTH [13] is adopted in this study. The peak average displacement in time history $\bar{w}_{max}$, is plotted against the load, where the average displacement $\bar{w}$ is given by

$$\bar{w}=\int_0^a 2\pi rw dr \Big/ \int_0^a 2\pi r dr = 2\int_0^1 \rho w d\rho = \sum_{m=1}^{N+3} \frac{2}{m+1} a_m. \tag{3.6}$$

If there is a load where a sharp jump in $\bar{w}_{max}$ occurs for a small change in the load amplitude, than this load is taken as the buckling load. If, on the other hand, there is gradual transition from low to the high range of w_{max}, the buckling load is taken as the load corresponding to the lower knee of the $\bar{w}_{max}$ versus P curve [6,10].

3.2. Static buckling

The average deflection is incremented in small steps and the first maximum in the curve of P versus $\bar{w}$ is taken as the static buckling load. However, if the solution fails to converge in 100 iterations, the corresponding load is also taken as the buckling load.

4. RESULTS AND DISCUSSION

The results are presented for static and dynamic buckling of isotropic ($\beta=1$) and orthotropic ($\beta=3$) shallow spherical caps with values of shell parameters H/h from 2 to 10 for several values of initial imperfection. Uniformly distributed static and step pressure loading have been considered. Poisson's ratio has been taken as $\nu_\theta=0.3$ in all cases. Convergence studies, not being reported for brevity, have revealed that up to nine collocation points and $\Delta\tau=0.002$ are sufficient for accurate results.

The effect of initial imperfections on the static load deflection response of an orthotropic cap with $H/h=4$ and $\beta=3$ is shown in Fig. 2. The buckling loads decrease with an increase in initial imperfection. The static buckling loads of shallow spherical caps are plotted in Fig. 3 for $\beta=1$ and 3 for $w_{i0}=0.0, 0.1, 0.3$ and 0.5. The results of BUDIANSKY [1] for perfect isotropic caps and of KAO *et al.* [10] for isotropic caps with initial imperfections for $\lambda=5$ are also shown in Fig. 3 for comparison. The present results are in good agreement with these results for the isotropic cap. It can be observed from Fig. 3 that the qualitative pattern of results is not affected by initial imperfections but quantitatively there is a drastic reduction in buckling loads with initial imperfection.

The effect of initial imperfection on the dynamic buckling is analysed for uniformly distributed step pressure load. The typical average deflection response to step load for an orthotropic shell with $H/h=10$, $w_{i0}=0.3$ and $\beta=3$ is given in Fig. 4 for two values of step pressure. The maximum average deflection has a sharp jump

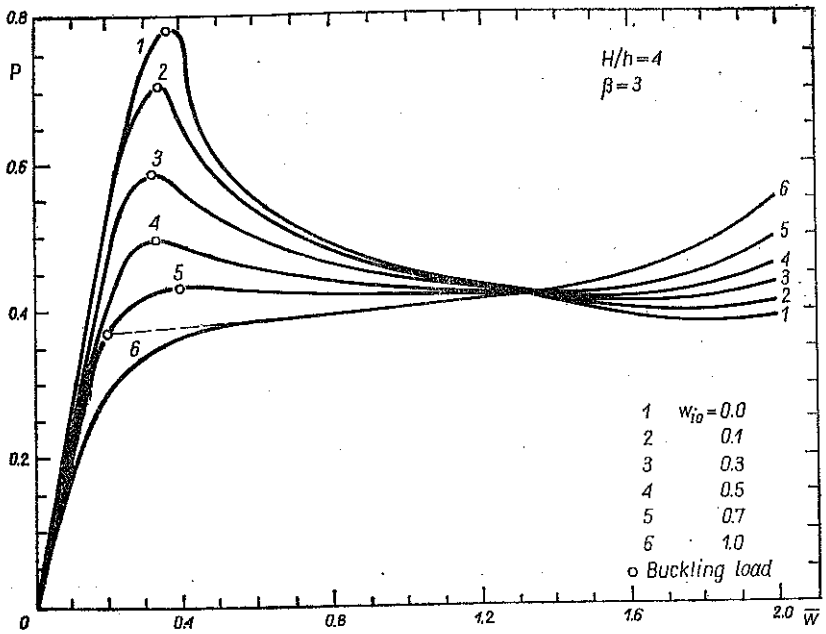

FIG. 2. Effect of initial imperfections on the static load deflection response of an orthotropic cap with $H/h=4$ and $\beta=3$.

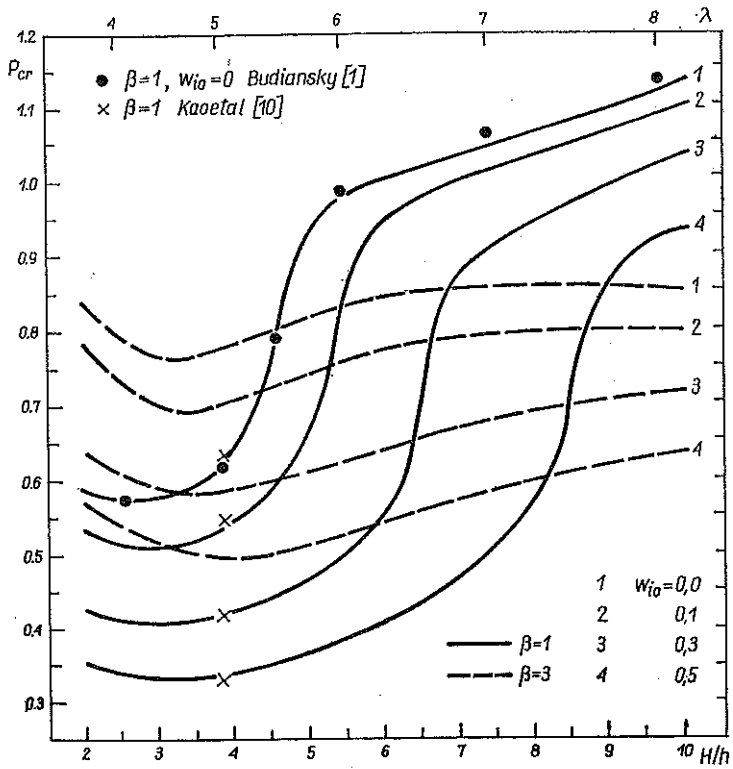

FIG. 3. Effect of initial imperfections on static buckling loads.

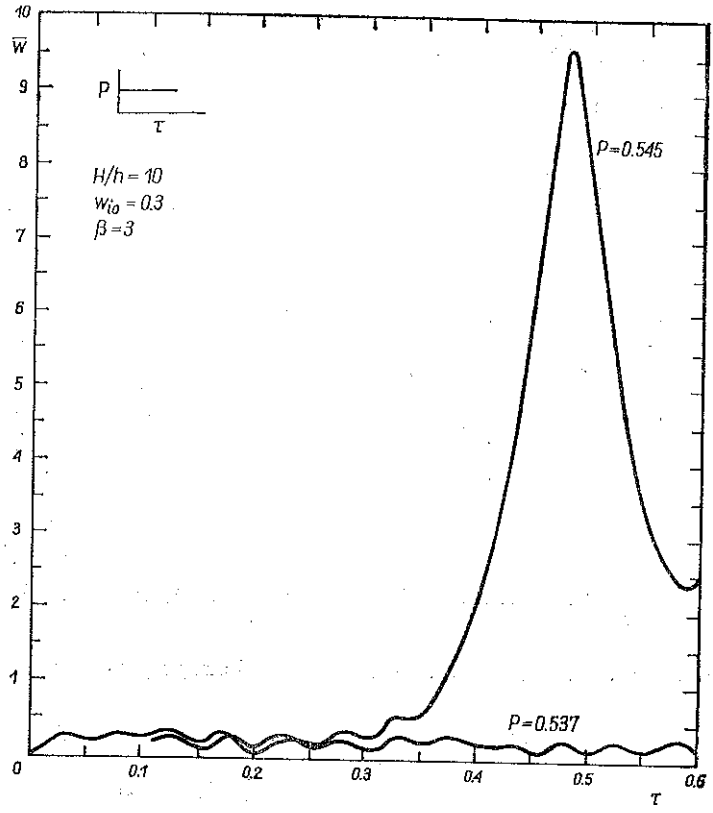

FIG. 4. Average deflection response to step load (H/h=10, w_{i0}=0.3, β=3).

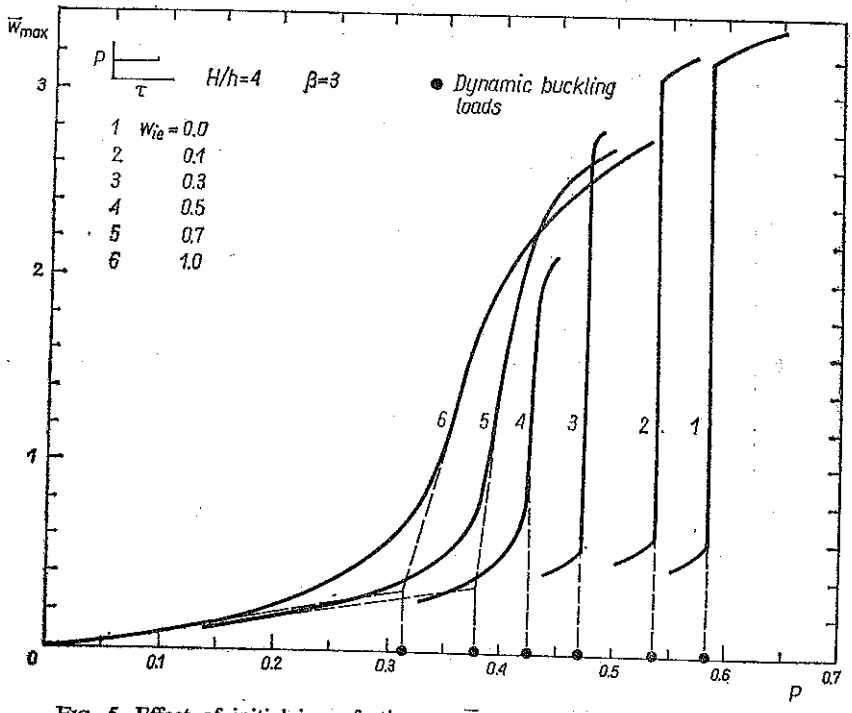

FIG. 5. Effect of initial imperfection on $\bar{w}_{max}$ vs P curve (H/h=4, β=3).

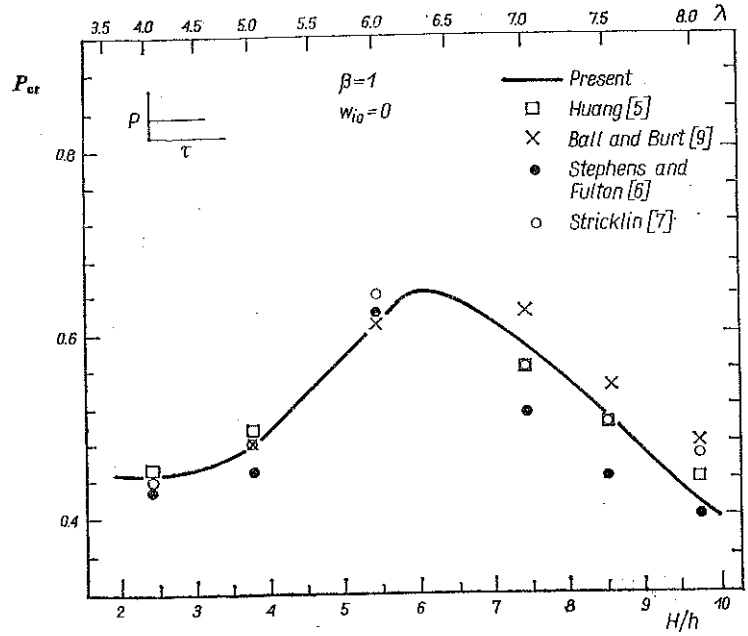

FIG. 6. Comparison of dynamic buckling loads for isotropic perfect spherical caps.

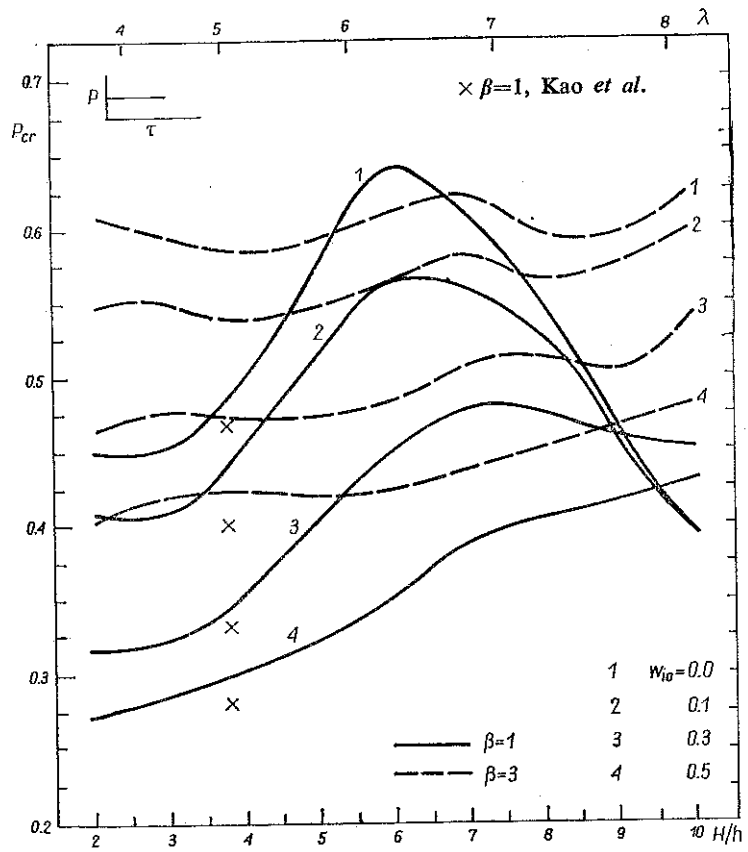

FIG. 7. Effect of initial imperfection on dynamic buckling loads.

when P is increased from 0.537 to 0.545. The effect of initial imperfection on w_{max} versus P curve is shown in Fig. 5 for a cap with $H/h=4$ and $\beta=3$. It can be noted from Fig. 5 that for smaller values of w_{i0} the buckling load corresponds to the sharp jump in the curve whereas for larger values of w_{i0} the buckling load corresponds to the lower knee of the curve.

In order to have a further check on the procedure the present results for an isotropic perfect cap are compared with the available results in Fig. 6. It can be seen that the present results fall within the range of the results reported by other researchers and are in close agreement with some of them. The dynamic buckling loads for $\beta=1$ and 3 are given in Fig. 7 for $w_{i0}=0.0$, 0.1, 0.3 and 0.5. The initial imperfections have little effect on the qualitative variation of P_{cr} with H/h but there is a drastic reduction in the buckling load with increase in initial imperfection. For comparative evaluation of the effect of w_{i0} on static and dynamic buckling loads, P_{cr} is plotted against the imperfection w_{i0} for caps with $H/h=4$ and 8 and $\beta=1$ and 3. It is evident from Fig. 8 that initial imperfections reduce shell buckling capacity at a faster rate for static loading than for the dynamic case.

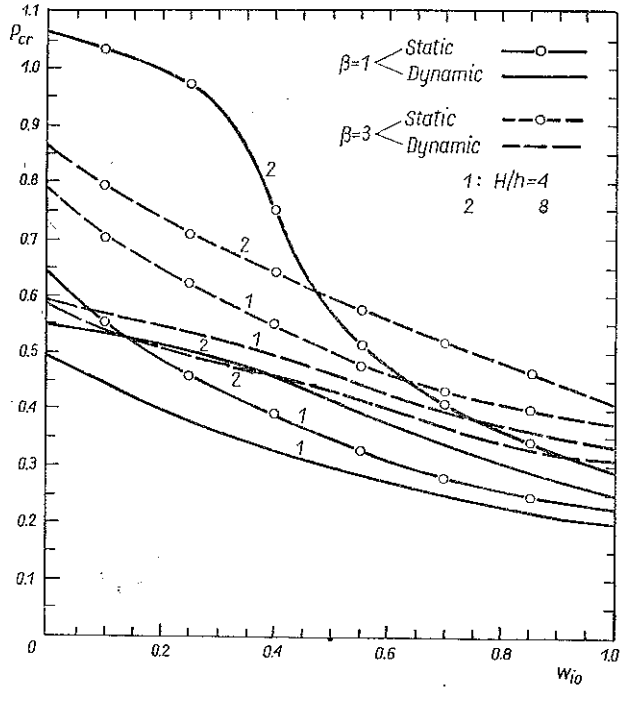

FIG. 8. Static and dynamic buckling loads vs initial imperfection.

The new results reported herein for orthotropic caps with initial imperfections using the simple and efficient method of orthogonal point collocation are of interest to the designers of these shell structures with initial imperfections due to manufacture and assembly.

REFERENCES

1. B. BUDIANSKY, *Buckling of clamped shallow spherical shells*, Proc. IUTAM, Symp. on Theory of Thin Elastic Shells, Delft, The Netherlands, Ed. W. T. KOITER, 64—94, 1959.
2. G. A. THURSTON, F. A. PENNING, *Effect of axisymmetric imperfections on the buckling of spherical caps under uniform pressure*, AIAA J. **4**, 319—327, 1966.
3. J. W. HUTCHINSON, *Imperfection sensitivity of externally pressurized spherical shells*, J. Appl. Mech., **34**, 49—55, 1967.
4. T. KOGA, N. J. HOFF, *The axisymmetric buckling of initially imperfect complete spherical shells*, Int. J. Solids Struct., 1969.
5. N. C. HUANG, *Axisymmetric dynamic snapthrough of elastic clamped shallow spherical shells*, AIAA J. **7**, 215—220, 1969.
6. W. B. STEPHENS, R. E. FULTON, *Axisymmetric static and dynamic buckling of spherical caps due to centrally distributed pressures*, AIAA J., **7**, 2120—2126, 1969.
7. J. A. STRICKLIN, J. E. MARTINEZ, *Dynamic buckling of clamped spherical caps under pressure loadings*, AIAA J., **7**, 1212—1213, 1969.
8. M. UEMURA, *Axisymmetric buckling of an initially deformed shallow spherical shell under external pressuse*, Int. J. Nonlin. Mech., **6**, 177—192, 1971.
9. R. E. BALL, J. A. BURT, *Dynamic buckling of shallow spherical shells*, J. Appl. Mech., **40**, 411—416 1973.
10. R. KAO, N. PERRONE, *Dynamic buckling of axisymmetric spherical cap with initial imperfection*, Comput. and Struct., **9**, 463—473, 1978.
11. R. KAO, *Nonlinear dynamic buckling of spherical caps with initial imperfections*, Comput. and Struct., **12**, 49—63, 1980.
12. K. J. BATHE, E. L. WILSON, *Numerical methods in finite element analysis*, Prentice Hall, Inc., Englewood Cliffs, New Jersey 1976.
13. B. BUDIANSKY, R. S. ROTH, *Axisymmetric dynamic buckling of clamped shallow spherical shells*, NASA TND 1510, 597—606, 1962,

STRESZCZENIE

OSIOWO-SYMETRYCZNE WYBOCZENIE STATYCZNE I DYNAMICZNE MAŁOWYNIOSŁEJ ORTOTROPOWEJ POWŁOKI SFERYCZNEJ Z DEFEKTAMI WSTĘPNYMI

Defekt wstępny powłoki sprężystej ma postać zagłębienia osiowo-symetrycznego. Równania problemu wyrażono przez przemieszczenie normalne w i funkcję naprężenia ψ. Zastosowano metodę ortogonalnej kolokacji punktowej do dyskretyzacji przestrzennej oraz schemat Newmarka-β dla kroków czasowych. Rozważono przypadki ciśnienia równomiernego oraz obciążenia w postaci funkcji schodkowej. Rozwiązanie dla idealnie sferycznej powłoki pod obciążeniem przyłożonym skokowo pokrywa się dobrze z wcześniejszymi wynikami. Wpływ wstępnego defektu na wielkość statycznych i dynamicznych obciążeń krytycznych przeanalizowano dla stosunków wysokości do grubości powłoki sięgających wartości 10.

Резюме

ОСЕСИММЕТРИЧНЫЙ СТАТИЧЕСКИЙ И ДИНАМИЧЕСКИЙ ПРОДОЛЬНЫЙ ИЗГИБ ПОЛОГОЙ ОРТОТРОПНОЙ СФЕРИЧЕСКОЙ ОБОЛОЧКИ СО ВСТУПИТЕЛЬНЫМИ ДЕФЕКТАМИ

Вступительный дефект упругой оболочки имеет вид осесомметричного заглубления. Уравнения проблемы выражены через нормальное перемещение w и функцию напряжения ψ. Применен метод ортогональной точечной коллокации для пространственной дискрети-

зации и схема Ньюнарка-β для временных шагов. Рассмотрены случаи равномерного давления и нагрузки в виде скачкообразной функции. Решения для идеально сферической оболочки под нагрузкой приложенной скачкообразно совпадают хорошо с более ранними результатами. Влияние вступительного дефекта на величину статических и динамических критических нагрузок проализировано для отношений высоты к толщине оболочки, достигающих значения 10,

DEPARTMENT OF APPLIED MECHANICS
INDIAN INSTITUTE OF TECHNOLOGY, NEW DELHI, INDIA.

Received August 8, 1983.